2021

Thermodynamic Comparison of Magnetocaloric and Vapor Compression Domestic Wine Coolers

Natália Maleski de Sá
Federal University of Santa Catarina, Brazil

Alan Tihiro Nakashima
Federal University of Santa Catarina, Brazil, alan.nakashima@polo.ufsc.br

Jaime Andrés Lozano

Jader Riso Barbosa Jr.

Thermodynamic Comparison of Magnetocaloric and Vapor Compression Domestic Wine Coolers

Natália M. DE SÁ, Alan T.D. NAKASHIMA, Jaime A. LOZANO, Jader R. BARBOSA Jr.*

POLO - Research Laboratories for Emerging Technologies in Cooling and Thermophysics
Department of Mechanical Enginering, Federal University of Santa Catarina
Florianópolis, SC, Brazil
Phone: + 55 48 3721 7900, E-mail: jrb@polo.ufsc.br

* Corresponding Author

ABSTRACT

This paper presents a comparative study of magnetocaloric and vapor compression wine coolers. The vapor compression system is a commercially available 31-bottle climate class N appliance, whereas the magnetic cooling device is a TRL-5 prototype connected to the retrofitted insulated cabinet of the same VC cooler. Test procedures included temperature pull-down and standardized steady-state energy consumption tests. Detailed instrumentation of both systems allowed a low-level comparison in terms of first- and second-law based parameters that is unique in the literature. Although the vapor compression system is more efficient than the present magnetic cooling prototype, the behavior of its internally ideal *COP* led to significant, but realistic design improvements which were evaluated and quantified via a genetic algorithm-based optimization aimed at reducing the system mass and the power consumption. The numerical model, supported by the experimental data, indicate that magnetic cooling systems, although bulkier than their vapor compression counterpart, can be competitive in terms of thermodynamic performance.

1. INTRODUCTION

Mechanical vapor compression (VC) is the most widely used cooling technology. Despite its high efficiency and compactness, the use of environmentally harmful substances in VC systems is still a major concern. Among all not-in-kind cooling technologies, magnetic refrigeration (MR) is ranked as one with a very high potential to substitute VC in some applications (Brown & Domanski, 2014; Qian et al., 2016). Essentially, MR replaces the compression/expansion of a volatile fluid and its liquid-vapor phase-change refrigerating effect by the magnetization/demagnetization of a solid-state refrigerant going through a magnetic phase transition Despite the lower specific refrigerating effect of MR, the magnetocaloric effect (MCE) is reversible in some materials, which favors the thermodynamic efficiency.

Since the pioneering work of Brown (1976), whose device produced a temperature span of 47°C using a 7-T superconducting coil and gadolinium (Gd) plates as the magnetocaloric material (MCM), several lab-scale prototypes have been developed, most of them based on the active magnetic regenerator (AMR) cycle (Greco et al., 2019; Kitanovski, 2020). However, despite some notable advances, MR for near room-temperature applications still remains at a pre-commercialization stage (i.e., at low to intermediate levels of technology readiness), which often precludes a thorough comparison with VC for a particular application. In the literature, most comparative assessments of cooling technologies are performed at a high or intermediate level, and sometimes resort to mathematical models with variable degrees of complexity to quantify the relevant evaluation criteria (Qian et al., 2016; El Fil et al., 2021). To the present authors' best knowledge, no low-level assessment of MR in comparison to VC cooling has been performed so far. In this context, the goal of this paper is to experimentally evaluate the thermodynamic performance of VC and MR technologies when operating a wine cooler cabinet. While the VC system is a commercially available 31-bottle domestic wine cooler, the MR device is a state-of-the-art (TRL 5[1]) AMR prototype (Nakashima et al., 2021a) connected to the retrofitted cabinet of the same VC cooler.

To properly compare the different cooling technologies on the same thermodynamic baseline, first- and second-law based performance indexes are analyzed (Hermes & Barbosa, 2012). Temperature, pressure, power and torque measurements enable a direct quantification of internal losses, power consumption and external sources of irreversibility

[1] 9-point scale Technology Readiness Level (TRL) definitions: `www.nasa.gov/pdf/458490main_TRL_Definitions.pdf`

associated with finite temperature differences in the heat exchangers. The test procedures followed, as closely as possible, the recommendations of the IEC 62552 (2015) Standard, which was the first of its kind to establish a procedure to test wine coolers.

Finally, to guide the improvements needed to make the MR wine cooler more competitive in terms of efficiency and compactness, a lumped model of the MR system verified against the experimental data produced in this study was combined with a state-of-the-art genetic algorithm (GA) to optimize the AMR/magnet assembly geometric and operational parameters. The results indicate that the *COP* of the optimized MR wine cooler can be higher than that of the VC system, but the mass of the MR system is likely to be larger, even when achieving its minimum value is set as the objective function of the GA.

2. VAPOR COMPRESSION WINE COOLER

Vapor compression cooling is based on the mechanical compression and expansion of a volatile fluid. The compressor and the expansion device set the high and low pressures; at the low pressure, the refrigerant evaporates while extracting heat from the air inside the refrigerated cabinet and, at the high pressure, the refrigerant condenses while rejecting heat to the ambient. Some systems are equipped with an internal heat exchanger in which the refrigerant exiting the evaporator exchanges heat with the expanding fluid in the capillary tube. This reduces the quality of the two-phase mixture entering the evaporator (improving the refrigerating effect) and ensures a certain degree of superheat at the compressor inlet.

In the present study, the baseline product is a commercially available wine cooler, classified in the climate class N (subtropical). The insulated cabinet is divided into two compartments in which the temperature can be set individually between 8 and 18^{o}C by the onboard control system, according to the wine type. The product can store up to 31 bottles, 10 of them in the upper compartment and the remainder in the lower compartment. The refrigeration system of the wine cooler is charged with 38 g of R-134a and powered by a reciprocating, fixed speed compressor. The condenser is a wire-on-tube piece with 10 tube passes and 96 wires. Two roll-bond evaporators, one in each compartment, are connected to two distinct capillary tubes. The flow rate through each evaporator is controlled by a solenoid valve according to the temperature set point of each compartment. Two thermostats provide the input for the temperature control system, which employs an on-off control strategy. Figure 1 presents a schematic diagram of the system and a photograph of the product.

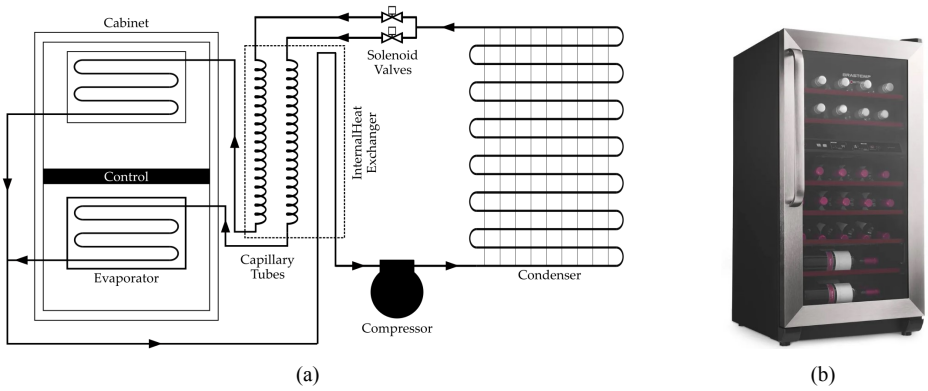

Figure 1: (a) Schematic diagram of the system and (b) photograph of the product.

2.1 Experimental Procedure

The tests conducted on the vapor compression wine cooler comprised an evaluation of the thermodynamic performance of individual components and of the system as a whole, including tests such as temperature pull-down time, annual energy consumption and reverse heat loss. To that end, the vapor compression wine cooler was instrumented with Type T thermocouples and a power transducer. Figure 2 presents the positions of the thermocouples assessing the air temperature inside the cabinet. The temperature of each compartment was determined by the average of two thermocouples in the upper compartment and three thermocouples in the lower compartment. The ambient temperature was computed as the average of three thermocouples placed at a distance of 30 cm from the cabinet external walls (left and

right) and from the glass door. Additional thermocouples were placed at the inlets and outlets of the condenser and of the two evaporators, with the hot junctions attached to the surfaces of those components, so as to avoid changing the original characteristics of the product.

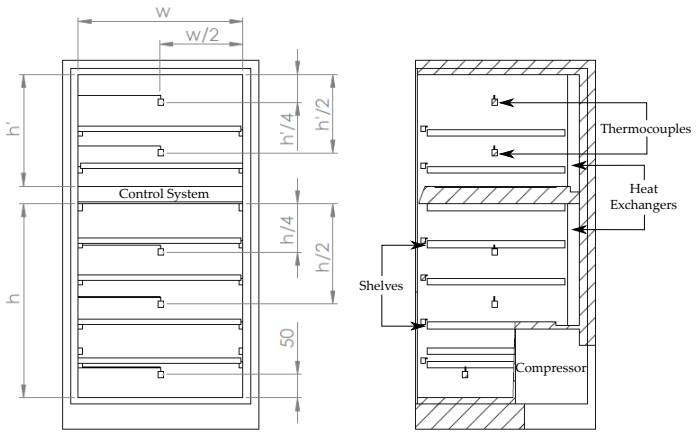

Figure 2: Temperature instrumentation of the cabinet for the tests of the vapor compression system (frontal and lateral view).

The tests were carried out in a climate-controlled test chamber, with air temperature and relative humidity control. The chamber is equipped with a vapor compression refrigeration system, an array of PID-controlled electrical resistances and a humidifier. The ambient temperature was kept at 25.0±0.5°C in all tests.

The temperature pull-down tests consisted of measuring the temperature decay inside the wine cooler compartments, from a state of thermal equilibrium (when the compressor is switched on), to the time temperature cycling (periodic steady state) begins. Tests were carried out for two different cabinet temperature set points: one with both thermostats set to the minimum operation temperature, 8°C, and another with both thermostats at the temperature recommended by IEC 62552 (2015) for wine coolers, 12°C.

The annual energy consumption test was carried out according to Thiessen et al. (2018), who proposed a simpler, yet reliable version of the energy consumption test recommended by IEC 62552 (2015). The procedure consisted of monitoring the power consumption of the system at periodic steady state for 5 hours, comprising a number of on-off compressor cycles. Defrost cycles were disregarded and the refrigerated compartments were empty (no bottles). The annual energy consumption test was carried out for internal (cabinet air) temperatures of 12°C, as indicated by IEC 62552 (2015), and 8°C.

Reverse heat loss (RHL) tests were performed to quantify the overall thermal conductance of the cabinet (Melo et al., 2000). The procedure consists of using electrical resistances to heat the air inside the cabinet of the (unplugged) refrigerator. Once the steady state is reached, the temperatures inside the compartment and the surroundings are recorded together with the power consumption of the electrical resistances. In total, four tests were conducted, each one with different compartment temperatures. The cabinet overall thermal conductance, UA_{cab}, was assessed by applying the data from the RHL tests in an energy balance over the wine cooler cabinet:

$$UA_{up}(T_{up} - T_{amb}) + UA_{low}(T_{low} - T_{amb}) = \dot{W}_{up} + \dot{W}_{low} \tag{1}$$

where $\dot{W}_{up}$ and $\dot{W}_{low}$ are the average power dissipation rates of the electrical resistances in the upper and lower compartments. The RHL test results were such that $UA_{cab} = UA_{up} + UA_{low} = 0.69 + 1.05 = 1.74 \pm 0.08$ W/°C.

2.2 Thermodynamic Analysis

The thermodynamic performance of the VC wine cooler is evaluated in terms of the coefficient of performance, *COP*, and the overall second-law efficiency, η_{2nd}, which can be split into internal and external contributions, $\eta_{2nd,i}$ and $\eta_{2nd,e}$,

respectively. The *COP* is defined as the ratio of the cooling capacity, $\dot{Q}_C$, to the average electric power consumption, $\dot{W}_{Total}$:

$$COP_{VC} = \frac{\dot{Q}_C}{\dot{W}_{Total}} \tag{2}$$

where, at steady state, $\dot{Q}_C = UA_{up}(T_{amb} - T_{up}) + UA_{low}(T_{amb} - T_{low})$. $\dot{W}_{Total}$ is calculated as the average of the product of the voltage and the electrical current at steady state. The overall second-law efficiency, η_{2nd}, and its internal and external contributions, $\eta_{2nd,i}$ and $\eta_{2nd,e}$, are calculated as follows:

$$\eta_{2nd} = \frac{COP}{COP_{Carnot}} \tag{3}$$

$$\eta_{2nd,i} = \frac{COP}{COP_{ii}} \tag{4}$$

$$\eta_{2nd,e} = \frac{COP_{ii}}{COP_{Carnot}} \tag{5}$$

where the Carnot *COP* and the internally ideal *COP* are defined as:

$$COP_{Carnot} = \frac{T_{cab}}{T_{amb} - T_{cab}} \tag{6}$$

$$COP_{ii,VC} = \frac{T_{evap,in}}{T_{cond,in} - T_{evap,in}} \tag{7}$$

where T_{cab} is the average cabinet temperature between the upper and lower compartment[2] and $T_{evap,in}$ and $T_{cond,in}$ are the average inlet temperatures of the evaporator and condenser [3], respectively.

3. MAGNETIC WINE COOLER PROTOTYPE

To date, most MR prototypes are based on the thermo-magnetic Brayton cycle with active regeneration and permanent magnet circuits. The active magnetic regenerator (AMR) is a porous bed of MCM capable of generating a temperature span several times greater than the adiabatic temperature change of the MCM, ΔT_{ad}. Through cyclic operation comprising magnetization and demagnetization of the AMR and the displacement of a fluid that acts as a thermal exchange medium between the solid refrigerant and the cold and hot reservoirs, a refrigerating effect (cooling capacity) is produced for a given temperature span (Trevizoli & Barbosa, 2020).

The magnetic wine cooler prototype developed in the present project is represented schematically in Fig. 3 (Nakashima et al., 2021a). The heat transfer fluid is a 10/90 vol.% solution of ethylene glycol with anti-corrosion additives in deionized water. The AMR/magnet assembly comprises the permanent magnet circuit and drive mechanism, 8 stationary AMR beds and flow distributors (manifolds). The magnetic circuit is composed of blocks of Nd-Fe-B (neodymium-iron-boron) and soft magnetic material (steel), and generates two regions of high magnetic field of about 1 T and two regions of low magnetic field of about 0 T as it rotates around the fixed AMR beds driven by an electric motor. The beds are filled with 2.25 kg of Gd and Gd-Y (gadolinium-yttrium) spheres, divided in three layers with different Curie temperatures. The variable speed liquid pump and a set of 8 solenoid valves (to direct the fluid flow to the appropriate AMR bed) are positioned at the hot side, where three fan-supplied finned tube heat exchangers (HHEx) mounted in parallel are responsible rejecting heat to the ambient without raising the internal fluid side pressure drop. The cold side comprises a fan-supplied finned tube heat exchanger (CHEx) mounted inside the wine cooler cabinet. A short video illustrating the main features of the system is available online[4].

[2] The average cabinet temperature was calculated as the weighted average based on the percentage volume of each compartment, 30 and 70% for the upper and lower compartment, respectively.

[3] $T_{evap,in}$ and $T_{cond,in}$ were assumed equal to the surface temperatures measured at the inlet of each component.

[4] `https://www.youtube.com/watch?v=y56ApAvZDoA`

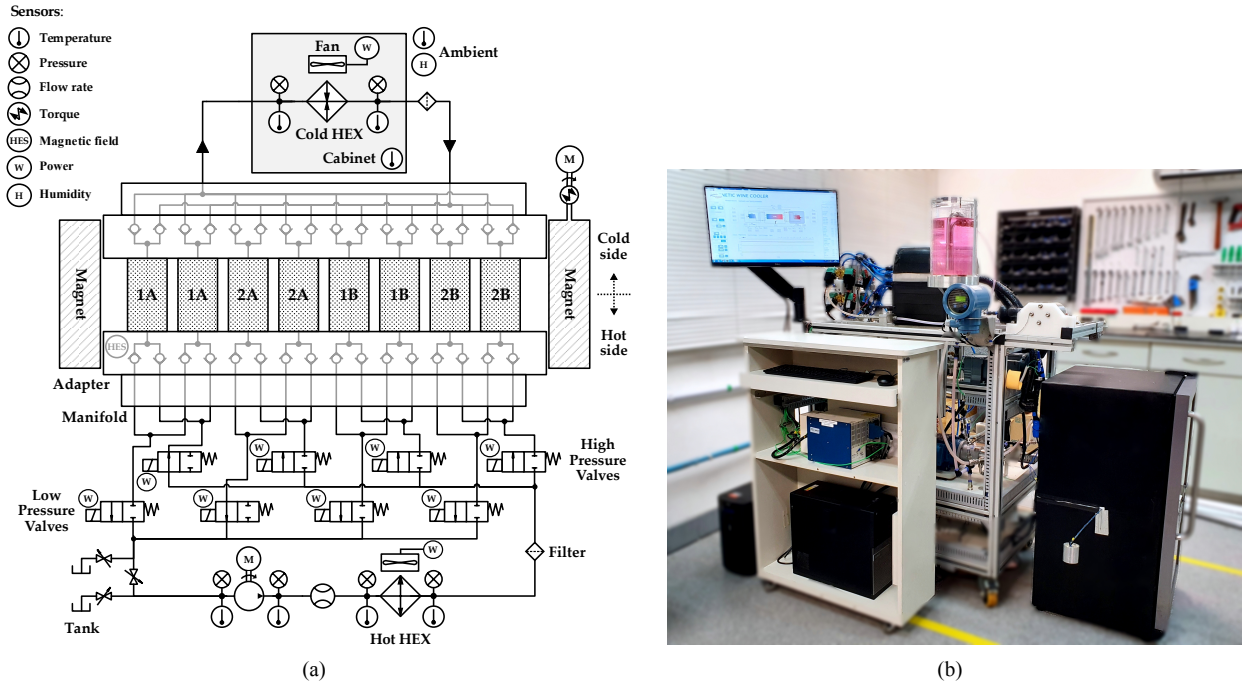

Figure 3: (a) Schematic diagram of the magnetic cooler prototype, (b) Photograph of the system and retrofitted cabinet.

3.1 Experimental Procedure

The original refrigerant circuit shown in Fig. 1 was replaced by a simpler one (single loop, one compartment) as the insulated cabinet was connected to the magnetic cooling system using a single cold heat exchanger. Figure 4 presents the positions of the thermocouples assessing the air temperature inside the retrofitted cabinet. The temperature of the air inside the cabinet, T_{cab}, was determined as the average of three Type T thermocouples. The ambient temperature, T_{amb}, was determined as described in Section 2.1. Other sensors included a turbine flow meter (liquid flow rate), torque transducer, Hall effect sensor (magnetic field) and absolute pressure transducers. The tests were carried out in a room where the ambient air temperature was controlled by a split-type air conditioner equipped with a variable speed compressor.

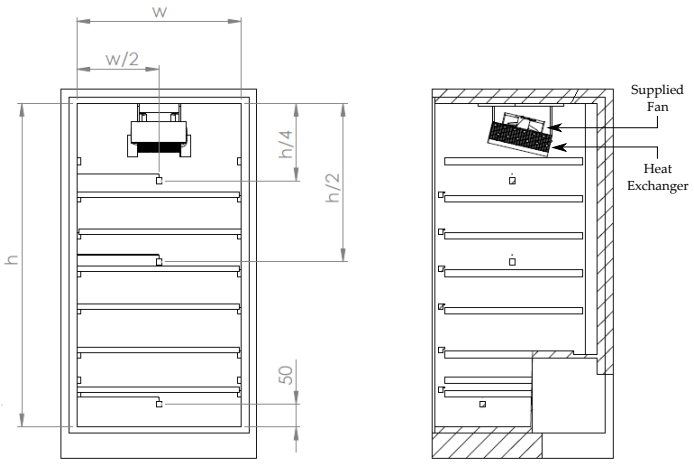

Figure 4: Temperature instrumentation of the retrofitted cabinet connected to the magnetic wine cooler prototype (frontal and lateral view).

The independent (input) variables of the tests were the cycle frequency (0.5, 0.75 and 1 Hz) and the fluid flow rate (125 to 225 L/h, in steps of 25 L/h). Combinations of the two input variables generated fifteen test conditions. The blow fraction[5] was kept fixed at 25%, the CHEx and HHEx fans operated at 3000 rpm, and the ambient temperature was controlled at 25±1°C. The dependent (output) variables were the thermal fluid temperature at various points of the hydraulic circuit (Fig. 3), the cabinet air temperature, and the power consumption of valves, fans, pump and magnet drive.

The performance tests begin with the cabinet and the ambient at thermal equilibrium. The AMR cycle is initiated as the motor, liquid pump, valves and HHEx fans are switched on and the fluid temperature starts to decrease. The CHEx fan remains initially off, but is immediately switched on as the liquid temperature stabilizes. As the system reaches steady state, the signals are recorded, enabling the computation of the *COP*, second-law efficiency, steady-state (average) cabinet temperature and power consumption. Of the fifteen tests, two conditions were selected as the best operating points for further temperature pull-down tests: one which provided the minimum steady-state cabinet temperature and another which gave the best thermodynamic performance.

3.2 Magnetic Wine Cooler Thermodynamic Analysis

As with the VC system, the thermodynamic performance of the magnetic wine cooler was evaluated in terms of the *COP*, second law efficiency, η_{2nd}, and its internal and external contributions, $\eta_{2nd,i}$ and $\eta_{2nd,e}$. The *COP* is defined as:

$$COP_{MR} = \frac{\dot{Q}_{load} + \dot{W}_{CF}}{\dot{W}_{P} + \dot{W}_{Mo} + \dot{W}_{CF} + \dot{W}_{HF} + \dot{W}_{V}} \tag{8}$$

where $\dot{Q}_{load} = UA_{cab}(T_{amb} - T_{cab})$. The power consumption of the pumping system is estimated from the viscous dissipation rate, for a pump efficiency of 21% (based on the manufacturer data) as follows:

$$\dot{W}_{P} = \frac{\dot{V}(p_{out} - p_{in})}{\eta_{P}} \tag{9}$$

The power consumption of the magnet rotating system is calculated as follows, also with an electrical motor efficiency of 81% (based on the manufacturer data):

$$\dot{W}_{Mo} = \frac{2\pi f \Gamma}{\eta_{M}} \tag{10}$$

The power consumption of the CHEx and HHEx fans and valves are calculated based on current and voltage measurements. The Carnot *COP* is calculated as in Eq. (6) and the internally ideal *COP* of the magnetic system is given by:

$$COP_{ii,MR} = \frac{T_{CHEx,in}}{T_{HHEx,in} - T_{CHEx,in}} \tag{11}$$

where $T_{CHEx,in}$ and $T_{HHEx,in}$ are the average temperatures at the inlets of the CHEx and HHEx, respectively. The overall, internal and external second-law efficiencies are calculated as previosly presented in Eqs. (3)-(5).

4. PERFORMANCE COMPARISON

Both VC and MR technologies were compared with respect to their performances when operating the same refrigerated cabinet. In order to establish a baseline, the performance metrics were evaluated as a function of the steady-state cabinet temperature. Figure 5(a) presents the *COP* as a function of the cabinet temperature for all test conditions. The first striking feature is the low value of COP_{VC}, around 0.7, which is about half the normally expected for typical household refrigerators. This is due to an oversized compressor, certainly not selected to maximize the energy efficiency of the

[5]The blow fraction is the ratio of the blow period in one regenerator and the total cycle period.

product. For the MR prototype, the *COP* decreases with the flow rate for the three frequencies as a result of the much more significant increase of the fluid pumping power in comparison with the cooling capacity. Also, the prototype reached a minimum steady-state cabinet temperature of 10.8°C, and its best *COP* was 0.41, which is about 40% lower than the *COP* of the VC wine cooler (~0.7) for a similar cabinet temperature (~12°C). In terms of power consumption, the cost to lower the cabinet temperature from 12.5 to 10.8°C for the MR prototype was far greater than for the VC wine cooler to reduce the cabinet temperature from 12.0 to 8.2°C. In other words, the *COP* of the magnetic system went from 0.41 to 0.23, a reduction of 44%, while for the VC wine cooler the *COP* dropped from 0.70 to 0.68, only 3%, for a much more significant temperature decrease. Overall, the *COP* results for the MR system were clearly lower than the corresponding results for the VC wine cooler. Figure 5(b) presents the corresponding second-law efficiency results. Similarly, the second-law efficiency results of the magnetic prototype decrease with the flow rate for the three frequencies, and are all lower than the corresponding VC results. The best second-law efficiency of the MR prototype was 1.7%, about 46% lower than the second-law efficiency of the VC wine cooler for a similar cabinet temperature (~12°C), i.e., 3.1%.

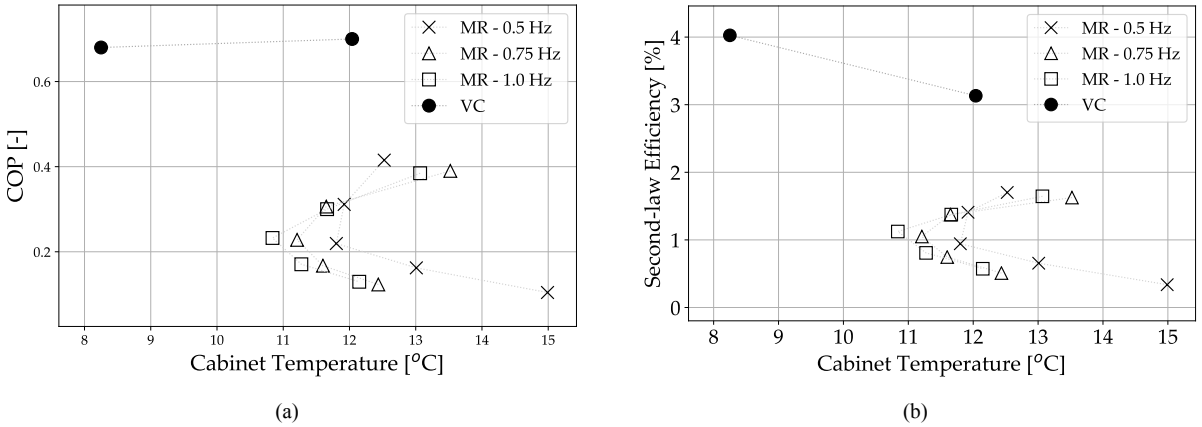

Figure 5: Results of (a) *COP* and (b) second-law efficiency as a function of the cabinet temperature.

For a more thorough evaluation of the cooling technologies, the best performing point of the MR prototype (f = 0.5 Hz, $\dot{V}$ = 125 L/h), which resulted in a cabinet temperature of 12.5°C, is compared with the 12.0°C set point condition of the VC system. Figures 6(a) and (b) present the values of *COP* and second-law efficiency of the magnetic prototype and VC wine cooler for these test conditions. Although the actual *COP* of the magnetic cooling prototype was about 40% lower than the actual *COP* of the VC system, its internally ideal *COP* was more than two times higher than the internally ideal *COP* of the VC device. The outcome of theses results is twofold. First, it reveals how much greater the internal losses in the magnetic system are in comparison with the VC cooler. Indeed, this is confirmed by the fact that the internal second-law efficiency of the VC system is almost four times higher. Second, the values of the internally ideal *COP* reflect the use of forced convection heat exchangers in the magnetic cooler, which had to be installed in order to attenuate the impact of the internal losses in the MR system on its overall performance. Nevertheless, as will be discussed below, there is much room for improving the efficiency of the magnetic cooler, for instance, by using first-order MCMs (which exhibit larger values of the MCE than the currently used alloys) and reducing friction losses. Again, the use of fan-assisted compact heat exchangers in the magnetic cooler prototype gives rise to an external second-law efficiency roughly two times higher than that of the vapor compression system, which employs natural draft condenser and evaporators.

Clearly, the lower values of *COP* and η_{2nd} of the magnetic prototype were due to a higher energy consumption, which was approximately 94% higher (505 kWh/year) than the annual energy consumption of the vapor compression wine cooler (272 kWh/year). Further analyses indicated that friction in the liquid pump was the main source of irreversibility in the magnetic wine cooler prototype, being responsible for about 50% of the total power consumption and 45% of total entropy generation at the best performance condition. As for the temperature pull-down time, the magnetic prototype reached steady-state in 5 h, almost 5 times greater than the time taken by the vapor compression system (1.1 h). Nevertheless, the magnetic system pull-down time can be reduced with the implementation of control strategies to determine the best flow rate and frequency combination. Similar strategies can also improve the overall performance.

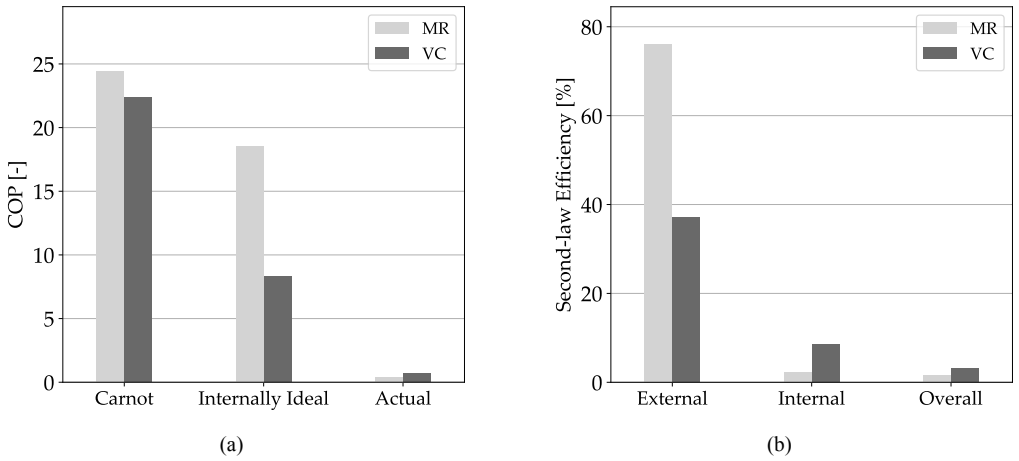

Figure 6: Breakdown of the figures of (a) *COP* and (b) second-law efficiency.

Table 1 summarizes the main performance parameters of the two systems for a steady-state cabinet temperature around 12°C.

Table 1: Comparison of the main performance parameters of the vapor compression cooler and magnetic prototypes for a cabinet temperature around 12°C.

Parameters	**Cooling Technology**	
	Vapor compression	Magnetic
Average cabinet temperature [°C]	12.0 ± 0.1	12.5 ± 0.1
Cooling capacity [W]	22.2 ± 1.4	24.3 ± 1.2
Energy consumption [kWh/year]	272 ± 46	505 ± 22
COP [-]	0.70 ± 0.15	0.41 ± 0.04
Overall η_{2nd} [%]	3.1 ± 0.9	1.7 ± 0.2
Pull-down time [h]	1.1	5.0

5. MAGNETIC SYSTEM OPTIMIZATION

Even though the MR system was not able to achieve efficiencies comparable to those of the VC wine cooler, the results indicate that optimization strategies coupled with some design modification can help to reduce the thermodynamic losses. In this sense, the present data were used to validate a new model of magnetic refrigeration systems (Nakashima et al., 2021b) aiming to identify and evaluate possible improvements. The model is divided into five sub-models: (i) a lumped thermal-hydraulic AMR model, (ii) an algebraic model of the magnetic field change, (iii) an empirical model for the pump, (iv) an effectiveness-*NTU* model for the heat exchangers, and (v) a lumped thermal model for the cabinet. For simplicity, only the AMR, magnetic field and cabinet sub-models (with UA_{cab} replacing the thermal resistance network in the latter) were considered in the GA optimization problem, which was solved using the Non-dominated Sorting Genetic Algorithm II (NSGA-II).

Two objective functions were considered in the GA optimization: minimum system mass and minimum overall power consumption. The input parameters were the magnet and AMR dimensions, flow rate, frequency and blow fraction. The constraint was the cooling capacity, which could not be lower than that produced by the MR system in the 12°C tests (see Table 1). The ambient temperature was kept fixed at 25°C. It was assumed that the regenerator temperature span was 3°C larger than the system temperature span (difference between the ambient and cabinet temperatures) to account for external losses in the heat exchangers. The AMR beds were composed of eight layers of first-order La-Fe-Si (lanthanum-iron-silicon) alloys (Vieira et al., 2021) with equally distributed transition temperatures over the temperature span. In this more compact configuration, which uses a solid-state refrigerant with a first-order MCM, a double-effect piston pump is considered, eliminating the need for solenoid valves. A realistic value for the overall pump was estimated at 30%.

Figure 7 shows the *COP* as a function of the system mass for the VC and MR systems considering a 12°C cabinet temperature. The black circle and cross markers represent the tests described in Section 4, while the grey circles are the Pareto front obtained from the GA optimization. The points at the ends of the front are the minimum mass and minimum power systems. The first general remark is that the efficiency of any optimal MR system can surpass that of the VC system tested in this work. For instance, even the minimum mass optimum MR system reached a *COP* of 1.3, which is 86% higher than the VC wine cooler. However, a second point arises when looking at the masses of the systems: the minimum mass achieved by the MR system was 24 kg, which is much more than the 9 kg of the VC cooler. This fact is directly linked to the lower value of the specific refrigerating effect of MR, which is associated with a solid-state phase transition. The larger mass translates into a higher initial cost of the product, which can be compensated by lifetime savings in energy consumption. Potentially, the highest *COP* of the optimized MR system can be as high as 1.9, which is 171 % above the commercial system. Further optimization of the magnetic circuit can certainly contribute to reducing the system volume, and this has been the focus of current research. Also, future comparisons will consider more efficient commercially available VC appliances.

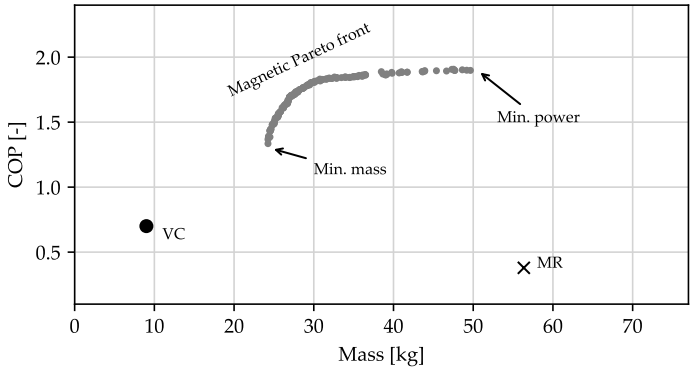

Figure 7: *COP* as a function of the system mass for the VC and MR coolers for a 12°C cabinet temperature. Pareto front of the MR system GA optimization.

6. CONCLUSIONS

A thermodynamic performance comparison of domestic wine coolers operated by magnetocaloric and vapor compression (VC) cooling systems was presented. Both systems were evaluated based on temperature pull-down behavior and steady-state energy consumption following, as closely as possible, the recommendations of the IEC 62552 (2015) Standard. First- and second-law performance indexes were used to quantify the internal and external losses at a 12°C cabinet temperature condition. Overall, the wine cooler was more efficient when operated by the VC system. The magnetic refrigeration (MR) prototype consumed almost twice the power to achieve around the same cabinet temperature, resulting in values of *COP* and η_{2nd} which were 40% and 46% lower than the VC system. Moreover, the VC system was almost 4 times more internally efficient than the MR prototype, indicating that there is still a lot to be improved in the latter system. For instance, the liquid pump was the least efficient component, being responsible for nearly 50% of the total power consumption. Nevertheless, the high internally ideal *COP* of the MR prototype pointing to a significant potential for improvement. Thus, to further evaluate this potential, some realistic design improvements, such as the use of a better pumping system and first-order magnetocaloric materials, were combined with a genetic algorithm optimization aiming at minimizing the system mass and the power consumption. The results pointed to MR systems which can be competitive in terms of efficiency, but are still bulkier than their VC counterparts because of the lower specific refrigerating effect of solid-state refrigerants.

NOMENCLATURE

COP	coefficient of performance	(-)	UA	overall thermal conductance	(W/°C)
f	frequency	(Hz)	$\dot{V}$	volumetric flow rate	(L/s)
p	absolute pressure	(kPa)	$\dot{W}$	power consumption	(W)
$\dot{Q}$	heat transfer rate	(W)	Γ	torque	(N · m)
T	temperature	(°C)	η	efficiency	(%)

Subscripts

C	cold side	int	internal
cab	cabinet	in	entering
CF	cold side fan	load	ambient thermal load
CHEx	cold side heat exchanger	low	lower compartment
cond	condenser	Mo	motor of the magnet
evap	evaporator	out	exiting
ext	external	P	pump
HF	hot side fan	up	upper compartment
HHEx	hot side heat exchanger	V	valves
ii	internally ideal	2nd	second-law

REFERENCES

Brown, G. V. (1976). Magnetic heat pumping near room temperature. *Journal of Applied Physics*, *47*, 3673–3680.

Brown, S. J., & Domanski, P. A. (2014). Review of Alternative Cooling Technologies. *Applied Thermal Engineering*, *64*, 252–262.

El Fil, B., Boman, D. B., Tambasco, M. J., & Garimella, S. (2021). A comparative assessment of space-conditioning technologies. *Applied Thermal Engineering*, *182*, 116105.

Greco, A., Aprea, C., Maiorino, A., & Masselli, C. (2019). A review of the state of the art of solid-state caloric cooling processes at room-temperature before 2019. *International Journal of Refrigeration*, *106*, 66–88.

Hermes, C. J., & Barbosa, J. R. (2012). Thermodynamic comparison of Peltier, Stirling, and vapor compression portable coolers. *Applied Energy*, *91*, 51–58.

IEC 62552. (2015). Household refrigerating appliances - characteristics and test methods - Part 1: General requirements. In *International Electrotechnical Commission.* Geneva.

Kitanovski, A. (2020). Energy applications of magnetocaloric materials. *Advanced Energy Materials*, *10*, 1903741.

Melo, C., da Silva, L., & Pereira, R. (2000). Experimental evaluation of the heat transfer through the walls of household refrigerators. In *Proceedings of the International Refrigeration and Air Conditioning Conference, Paper 502.*

Nakashima, A. T. D., Fortkamp, F. P., de Sá, N. M., dos Santos, V. M. A., Hoffmann, G., Peixer, G. F., … Barbosa, J. R. (2021a). A magnetic wine cooler prototype. *International Journal of Refrigeration*, *122*, 110–121.

Nakashima, A. T. D., Peixer, G. F., Lozano, J. A., & Barbosa, J. R. (2021b). A comprehensive lumped model for magnetic refrigeration systems. *Applied Thermal Engineering*, *in preparation*.

Qian, S., Nasuta, D., Rhoads, A., & Wang, Y. (2016). Not-in-kind cooling technologies: A quantitative comparison of refrigerants and system performance. *International Journal of Refrigeration*, *62*, 177–192.

Thiessen, S., Knabben, F. T., Melo, C., & Gonçalves, J. M. (2018). A study on the effectiveness of applying vacuum insulation panels in domestic refrigerators. *International Journal of Refrigeration*, *96*, 10–16.

Trevizoli, P. V., & Barbosa, J. R. (2020). Overview on Magnetic Refrigeration. In *Elsevier Reference Collection: Materials Science and Materials Engineering.* doi: 10.1016/B978-0-12-815732-9.00025-5

Vieira, B. P., Bez, H. N., Kuepferling, M., Rosa, M. A., Schafer, D., Plá Cid, C. C., … Barbosa, J. R. (2021). Magnetocaloric properties of spheroidal $La(Fe,Mn,Si)_{13}H_y$ granules and their performance in epoxy-bonded active magnetic regenerators. *Applied Thermal Engineering*, *183*, 116185.

ACKNOWLEDGEMENTS

This work was partially funded by the INCT (National Institutes of Science and Technology) Program (CNPq Grant No. 404023/2019-3; FAPESC Grant No. 2019TR0846). Additional funding was provided by CAPES (Talents for Innovation Program - Grant No. 88887.194773/2018-00) to J. Lozano. Financial support from EMBRAPII and NIDEC GA (formerly Embraco) is also acknowledged.